applied optics

Optimization and maximum potential of optical antennae in near-field enhancement

PingPing Chen,[1,2] Ju Liu,[1] Li Wang,[1] Kuijuan Jin,[1] Yan Yin,[3] and ZhiYuan Li[1]

[1]Laboratory of Physics, Chinese Academy of Science, Beijing 100190, China
[2]e-mail: chenpingping11@mails.ucas.ac.cn
[3]e-mail: yan.yin@aphy.iphy.ac.cn

Received 20 April 2015; revised 26 May 2015; accepted 27 May 2015; posted 28 May 2015 (Doc. ID 238139); published 18 June 2015

We investigate four types of gold nanoantennae (the monopole, the dipole, the cone-shaped, and the cone-bowtie antenna), under a fixed working wavelength. The finite-difference time-domain (FDTD) simulations show that the near-field enhancement values do not increase monotonously when the antennae sizes decrease, and optimization conditions vary with the antenna shapes. We also propose a distributed dipole ring model to analytically calculate the near field. The size condition for the strongest enhancement is the compromising result of the total radiated energy and the near-field distribution factor. Assuming the cone-bowtie antenna is the best for high enhancement, the maximum potential in near-field enhancement is 2×10^5 for a linear signal or 4×10^{10} for typical nonlinear signals. © 2015 Optical Society of America

OCIS codes: (240.6680) Surface plasmons; (240.6695) Surface-enhanced Raman scattering.

http://dx.doi.org/10.1364/AO.54.005822

1. INTRODUCTION

During the past decades several nanostructure-based methods were proposed to get near-field enhancement (NFE) signals, such as using metal nanoparticle aggregates [1,2], metal nanoparticle dimers [3], sharp metallic tips [4], gain-assisted metal nanorods [5], and so on. Those methods or techniques are related to the concepts of optical antennae, which are nanostructures designed to enhance the interaction between the optical electromagnetic wave and the structures [6]. The main and key advantages of using an optical antenna as a near-field probe are to convert the light from free space to nanoscale areas [7] and to highly enhance the local field at a sample location. Typical applications can be found in surface enhanced Raman scattering (SERS) [8–10] and tip-enhanced scattering [11,12]. In order to quantify the enhancement effect, researchers are using the NFE factor, proportional to the square of the electric field, and the G factor, proportional to the fourth power of the electric field, to describe the level of the enhancement. The value of the NFE factor is critical in the applications of the optical antennae, because this value not only directly decides the signal strength, but also normally decides the signal-to-noise ratio and spatial resolution in the field-enhanced near-field optics. Therefore, how to optimize and what is the maximum potential of the NFE factor of optical antennae are very important questions. The answers will help to improve the usage of optical antennae and understand their application limits.

In this paper, we use the finite-difference time-domain (FDTD) simulation to evaluate the near-field properties of four types—the monopole, the dipole [13], the cone shaped, and the cone bowtie—antenna, of gold nanoantennae working at an 800-nm excitation wavelength. Our result supports that there is an optimum size of an antenna for a certain excitation wavelength to obtain the best NFE factor. The optimization conditions vary with the antenna shapes. Our simulation for cone-shaped antennae shows an order of magnitude higher enhancement than infinite-sized metal tips, and suggests a way to further improve tip enhancement by fabricating nanosized cone-shaped antennae. We also introduce a distributed dipole ring approximation method, use the quasi-static theory, and analytically calculate the near-field of the monopole and cone-shaped antennae. This method offers significantly reduced calculation time and much better physical insights than numerical methods. The outcome from analytical calculation is consistent with the result of the FDTD simulation, and reveals that the optimization condition in size is the compromised result of the total radiated energy of the antenna and the near-field distribution factor. In terms of the values of the best enhancement factor, our simulation for the cone-bowtie antenna gives 2×10^5 for a linear signal (proportional to the square of the electric field) and 4×10^{10} for typical nonlinear signals (proportional to the fourth power of the electric field). Those best enhancement values might be the maximum potential of optical antennae in NFE when we consider that the cone-bowtie antenna is the best design for high enhancement.

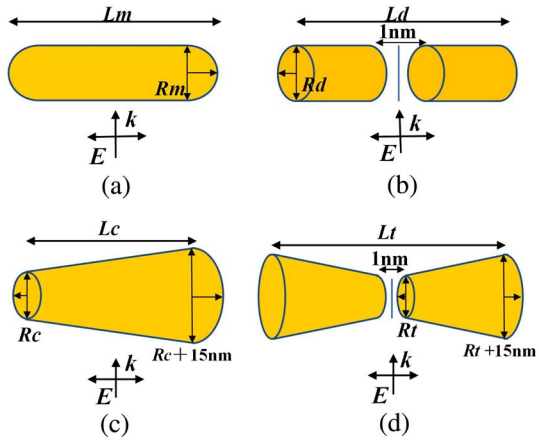

Fig. 1. Schematic pictures and dimensions of (a) the gold monopole antenna, (b) the gold dipole antenna, (c) the cone-shaped antenna, and (d) the cone-bowtie antenna.

2. NUMERICAL SIMULATION STEPS AND RESULTS

Four types of optical nanoantennae are considered in this work. The monopole antenna is a rounded cylindrical nanorod with hemispherical caps and the dipole antenna is a pair of nanorods with a 1-nm-wide gap. The cone-shaped antenna is a cone-like rod with a small end and a large end; the cone-bowtie antenna is a pair of cone-like rods arranged in a bowtie-like setting. Figure 1 shows the sketches of the antennae. L_m, R_m, L_d, R_d, L_c, R_c, L_t, and R_t are the total lengths and the tip radii of the monopole, dipole, cone-shaped, and cone-bowtie antenna, respectively. For cone-shaped and cone-bowtie antennae, the large end radii are maintained to be 15 nm larger than the tip radius. All four antennae are considered to be gold and placed in a vacuum. The polarization direction of the applied electric field is along the long axis of the antennae, and the propagating direction is in the perpendicular direction.

In this paper, we calculate the NFE values at a certain working wavelength of the four antenna types versus different radii using the FDTD method [14,15]. First, we set a series of different antenna radii and find the corresponding antenna lengths that make antennae resonant at 800 nm. We consider that an antenna is in best resonance with an 800-nm incident wave when its far-field extinction curve peaks at 800 nm, and assume that the condition for maximum NFE is approximately the same as the condition for maximum far-field extinction. In Table 1, we list all the investigated radii (R_m, R_d, R_c, and R_t from 2 to 30 nm) and the corresponding lengths (L_m, L_d, L_c, and L_t) found from our simulations for best working at 800 nm. All monopole, dipole, cone-shaped, and cone-bowtie antennae are evaluated at the 800-nm excitation wavelength. We use an optimization and parameter sweep function of the FDTD method to obtain the target antenna length for each radius. For an antenna radius, we know the rough length range for resonating at 800 nm from a published report [16]. The optimization function runs a large number of FDTD simulations with a sweeping antenna length within the known rough range, and gives us the target antenna length when the far-field extinction curve peaks at 800 nm. Next, based on these resonant structures, we use the FDTD simulation to calculate the antenna NFE factor, η (η_m, η_d, η_c, and η_t for the monopole, dipole, cone-shaped, and cone-bowtie antennae). η is the ratio of the near-field electric field square value to the incident electric field square value. The mesh sizes (the step sizes of the wave propagation) of the FDTD simulations are set to be 1/10 of the antenna radii. The amplitude of the near-field electric field is quantitatively calculated by taking an average of a monitor window that is 1 nm away from the tips of the monopole or cone-shaped antenna or is at the center of the gap of the dipole or cone-bowtie antenna. The size of the monitor window is the square of an antenna's diameter. Mathematically, we can write $\eta = \sum_i E_i^2 \times \text{mesh}^2/\text{monitor}$, where i is the mesh elements in the monitor window, E_i is the electric field in each mesh, mesh is the mesh size in length, and monitor is the area size of the monitor window for evaluating the near-field electric field. The amplitude of the incident field is considered to be 1.

Our simulation parameters and results are presented in Table 1. The subscripts m, d, c, and t identify the values for the monopole, dipole, cone-shaped, and cone-bowtie antenna, respectively. We also plot the curves of the NFE factors as functions of the radii for the antennae in Fig. 2, in order to offer a better viewing of the trend. Both from Table 1 and Fig. 2, our result shows that NFE has an optimized radius for all investigated antennae. The optimization conditions vary with the antenna shapes. For having the best NFE with an 800-nm excitation, this radius is 7 nm for the monopole and 5 nm for the dipole antenna. The cone-shaped antenna gives the best NFE at about 3 nm radius, and the cone-bowtie antenna appears to have the best NFE at or below 2 nm. The maximum enhancement factors are about 1.8×10^5, 4×10^4, 2.1×10^4,

Table 1. FDTD Simulation Parameters and Results for NFE Factors as Functions of the Antenna Radii

R (nm)	2	3	4	5	6	7	8	9	10	15	20	30
mesh (nm)	0.2	0.3	0.4	0.5	0.6	0.7	0.8	0.9	1.0	1.5	2	3
monitor (nm^2)	4 × 4	6 × 6	8 × 8	10 × 10	12 × 12	14 × 14	16 × 16	18 × 18	20 × 20	30 × 30	40 × 40	60 × 60
L_m (nm)	24.8	37.6	49.2	61	72	83.3	93.6	103.5	113.4	154.5	181	219.6
L_c (nm)	91.2	102	111	120	128	135.6	142	148	154	176	190.8	207
L_d (nm)	36.8	51.6	64.4	76	87.6	98	108	116.4	125	160	182	208.4
L_t (nm)	106	109.6	113.4	117	125	131	135	139	139.6	160	175	191.5
η_m	591	853	861	1136	1232	**1449**	1438	1391	1056	741	392	157
η_c	19,269	**21,282**	14,729	11,531	9710	7314	6793	4737	3778	1413	682	538
η_d	17,062	22,645	29,513	**38,796**	25,069	18,073	11,809	9067	8571	1845	525	161
η_t	**177,932**	127,824	58,811	30,465	29,863	23,409	23,474	15,145	11,660	2280	541	187

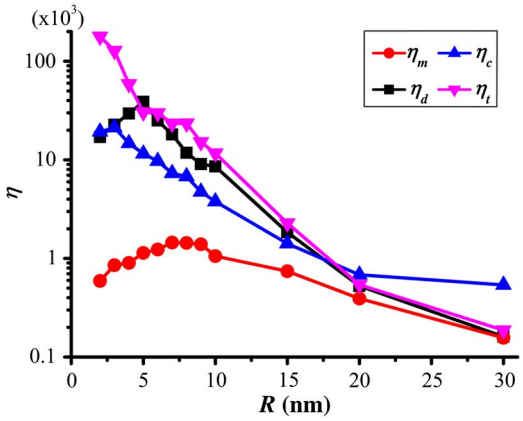

Fig. 2. Logarithm plots of NFEs of a monopole antenna (η_m, the red line with dot symbols), dipole antenna (η_d, the black line with square symbols), cone-shaped antenna (η_c, the blue line with triangle symbols), and cone-bowtie antenna (η_t, the pink line with reverse triangle symbols), as functions of their radii.

and 1.5×10^3 for cone-bowtie, dipole, cone-shaped, and monopole antennae, respectively.

It should be stressed that we use an approximation when we obtain the resonant antenna structures using the far-field extinction curve. We approximate that the condition for maximum NFE is the same as the condition for maximum far-field extinction. This approximation is not always valid for all cases, but holds well for the situation we consider here. In order to analyze the validity of this approximation, we present the spectral dependences of the far-field extinction curve and the NFE of a 10-nm radius monopole antenna in Fig. 3(a). We can see that the near-field resonant curve shifts slightly ($\Delta\lambda$) to a longer wavelength compared with the far-field extinction curve. For this monopole antenna, $\Delta\lambda = 3$ nm, $\lambda_{\mathrm{FWHM}} \approx 60$ nm, $\Delta\lambda/\lambda_{\mathrm{FWHM}} \approx 5\%$, and $\Delta\lambda/\lambda_c \approx 0.4\%$, where λ_{FWHM} is the full width at half-maximum (FWHM) of the resonant curves and λ_c is the center resonant wavelength. We also calculate the near-field and far-field resonance difference for an $R_d = 10$ nm dipole antenna as well. Our result gives $\Delta\lambda = 5$ nm, $\Delta\lambda/\lambda_c \approx 0.6\%$ for the dipole antenna. Both kinds of antennae show that the near-field and far-field resonance difference is numerically small enough compared to the FWHM of the resonant curves and the center wavelength so that the resonance condition difference between the near-field and far-field can be ignored within a 10% margin of error. Therefore, our approximation that the condition for maximum NFE is same as the condition for maximum far-field extinction is valid for the monopole and dipole antennae working around 800 nm.

We also need to discuss the effect of nonlocalization of the surface plasmon in the dipole and cone-bowtie antenna situations. When the gap between the two arms of the antennae is small enough (smaller than a few nanometers), the surface plasmon within the two arms becomes nonlocalized, will couple to each other. and does not have a clear cut boundary condition at the metal surface [17]. In principle, our FDTD simulation for the 1-nm gap dipole or cone-bowtie antenna is invalid for obtaining the accurate field enhancement factor. However, the purpose of the simulation for the dipole and cone-bowtie antennae is to find an upper limit for the field enhancement of optical antennae. The plasmon coupling between the two arms of the dipole antenna will only reduce the field intensity within the gap, so the true value of the enhancement factor will be smaller than that from our FDTD simulation. The value of the field enhancement factor from the FDTD simulation for the cone-bowtie antenna is valid as an upper limit to evaluate the potential of optical antennae in field enhancement applications.

We explored antenna radii down to 2 nm and gap size 1 nm, in order to find the best optimization conditions and maximum enhancement limitations. In terms of fabrication feasibility of corresponding dipole and cone-bowtie antennae, a 5-nm gap might be achievable by using a FIB (focused ion beam) quickly cutting through a connected two-arm antenna. For instance, using a FIB cuts the center of a nanorod with a diameter of a few nanometers to make a dipole antenna. How to achieve a 1-nm gap or make very sharp cone-bowtie structures remains an open question. However, we believe that the trends and behaviors for a 1-nm gap are valid for a 5-nm gap as well, and theoretical simulations can be a little bit ahead of experimental feasibility so that we can evaluate an experimental effort. The smallest 2-nm radius structure is getting close to the quantum regime, and whether the FDTD method still holds or partially holds is unclear. However, such a scale is also on the edge or outside of the maximum capability of the *ab inito* method. Considering the above reason and that the 2-nm data point is the edge data of our simulation, using the FDTD to simulate 2-nm radius structures is still a valid choice and the single point at 2 nm does not affect the overall trends and key findings.

3. ANALYTICAL CALCULATIONS WITH A DISTRIBUTED DIPOLE MODEL

We developed a distributed dipole model for analytically calculating the near field around a single body optical antenna. In this section, we will demonstrate this method's applications on monopole and cone-shaped antennae, and we will show that the physical reason of the resonant behavior of NFE versus radius is the compromise of two terms: the total radiated energy of the optical antenna and the near-field distribution factor. The size effect of metal nanostructure's interaction with light is dominated by different mechanisms for different structure sizes compared to the light wavelength. As in our case, the sizes of gold nanoantenna radii (2–30 nm) generally fit the quasi-static standard. In order to analytically explain the behavior of the NFE value changing with the antenna size, we build an approximate distributed dipole model based on electrostatic theory. We consider that the electric field around an antenna is the result of a two-step process. First, the incident wave interacts with, excites the antenna, and generates the polarization of the antenna. In this step, we take the nanoantenna as an ideal dipole and calculate its polarization under the electrostatic theory. Then, we consider the distribution of the surface charges with a dipole ring approximation. Using this model, we analytically calculate the NFE of gold monopole and

cone-shaped antennae and give the detailed steps for the monopole here.

Under the electrostatic theory, the nanoantenna can be approximately treated as an ideal dipole when its size is small compared with the incident wavelength and the polarization of the applied field is along the long axis [18]. Hence, the monopole antenna's far-field electromagnetic response to the applied uniform static electric field is mainly produced by this ideal dipole's excited oscillation. Because of energy conservation, the antenna's excitation level from the incident field can be described by this ideal dipole's polarizability. For simplicity, here we consider an ellipsoid with semi axes R, R, and $L/2$ to approximately substitute for our monopole antenna. The applied field propagates along the short axis and polarizes along the long axis. The polarizability of the gold monopole antenna can be presented as [19]

$$\alpha = \frac{2\pi R^2 L(\varepsilon - \varepsilon_0)}{3\varepsilon_0 + 3L_3(\varepsilon - \varepsilon_0)}, \tag{1}$$

where $L_3 = \frac{R^2 L}{4}\int_0^\infty \frac{dq}{((L/2)^2+q)f(q)}$, $f(q) = (q+R^2)(q+(\frac{L}{2})^2)^{\frac{1}{2}}$, and ε, ε_0 are the antenna's effective permittivity and vacuum permittivity at 800 nm, respectively. The dipole moment P, induced by the applied field, satisfies $P = \varepsilon_0 \alpha E_0$, where E_0 is the incident electric field. From Eq. (1), we can see that α has a resonance when the frequency and size-dependent dielectric function $\varepsilon(\omega, R)$ of the antenna fit the condition $|3\varepsilon_0 + 3L_3(\varepsilon - \varepsilon_0)| =$ Minimum. Here in our analytical model, the values of R and L of the antennae are taken from Table 1, the result of our FDTD resonance sweep. Therefore, the antennae with different diameters are all in resonance with the 800-nm excitation wavelength, and we are calculating their NFE factors analytically for comparison.

If an antenna size (i.e., radius) is larger than 25 nm, the contributions from higher-order multipoles and the phase retardation become important. The electromagnetic effect can be fully described by the bulk frequency-dependent dielectric constant [20] $\varepsilon(\omega)$. The nanoantenna size range in our work, mainly under 25 nm, is usually called as in the intrinsic regime,

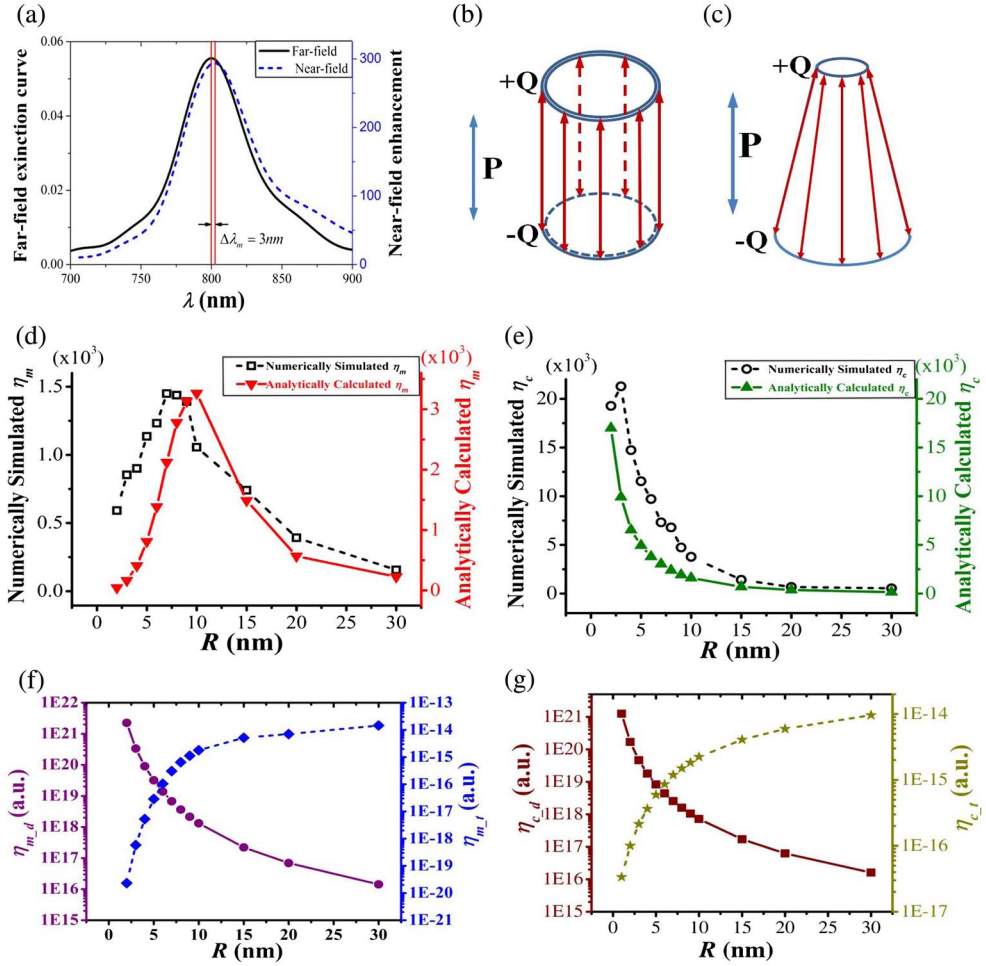

Fig. 3. (a) Far-field extinction curve (black line) and the NFE (blue dash line) spectral dependence of a gold monopole with a 10-nm radius; (b) and (c) are the schematics of the electron distribution in the dipole ring model for the monopole antenna and cone-shaped antenna, respectively; (d) and (e) are analytical and numerical NFE values versus the radius for the gold monopole antenna and cone-shaped antenna, respectively; (f) is the logarithm plots of η_{m_t} (blue dash line with diamond symbols) and η_{m_d} (purple solid line with dot symbols) versus the antenna radius for the monopole antenna; and (g) is the logarithm plots of η_{c_t} (yellow dash line with star symbols) and η_{c_d} (wine solid line with square symbols) versus the antenna radius for the cone-shaped antenna.

and the dipole plasmon oscillation determines the near-field properties. When a nanostructure's size reduces to a few nanometers, the excitation electric field exists both on the surface and in the internal of the structure. Therefore, a size-dependent dielectric function $\varepsilon(\omega, R)$ must be introduced to represent the electromagnetic and the optical properties of the antennae. For noble metals, in which there is a narrow forbidden energy band, the inter-band transitions must be taken into account, especially in the visible light frequency range [21]. Consequently, the dielectric function can be expressed as

$$\varepsilon = \left(\left(1 - \frac{\omega_p^2}{\omega^2 + i\omega\gamma}\right) + \chi_\infty\right)\varepsilon_0, \tag{2}$$

where the first part represented by the Drude model is the contribution of free electrons. $\chi_\infty = 9$ represents the interband transitions [22], ω is the frequency of the incident light, and ω_p is the plasma frequency, 1.36×10^{16} s^{-1} for gold [23]. γ is the collision frequency and becomes size-dependent because the additional collisions with particle boundaries increase the damping contribution. It can be written as [24]

$$\gamma = \gamma_{\text{bulk}} + A\frac{\nu_F}{a}, \tag{3}$$

where a is the particle radius, or the radius of the monopole antenna in our model. The parameter A is 1 for the simple Drude model and isotropic scattering, γ_{bulk} is the bulk collision frequency modified as $\gamma_{\text{bulk}} = \nu_F/l_\infty$, ν_F is the Femi velocity, and l_∞ is the conduction-electron mean free path. For gold, ν_F is 1.4×10^6 m/s and l_∞ is ~42 nm. We can get the specified monopole antenna polarizability by combining Eqs. (1), (2), and (3).

The near-field properties of a gold nanoantenna are determined by the charge accumulation on the antenna [25]. The surface charge oscillation plays an important role in localizing and enhancing the near field, which is originated from the resonant excitation. A monopole antenna cannot be simply regarded as an ideal dipole because the near-field location we are studying is too close to the surface of the antenna [26]. Here we establish a distributed dipole model to approximately describe the contribution of the surface charge oscillation in a monopole or cone-shaped antenna. Because of the edge effect, we approximately consider that the surface charges accumulate and oscillate around the rings of the end faces. The two rings formulate a dipole ring at the side face of the monopole or cone-shaped antenna, as Figs. 3(b) and 3(c) show. The near field is calculated by taking an average of the field in a monitor window, which is a round area ($4R^2$ in size and $1.13R$ in radius) and 1 nm away from the antenna end face. The monitor window in our analytical calculation has the same size in area as that in previous numerical simulation for the best comparability, but is round for the simplification in calculation. If the total charge of each ring is Q, the average electric field value within the monitor window of the monopole can be calculated as

$$\bar{E}^2 = \frac{Q^2}{64\pi^5\varepsilon_0^2 R^2}\int_0^R \left(\left(\sum\nolimits_j B_j\right)^2 + \left(\sum\nolimits_j C_j\right)^2\right)\cdot 2\pi r\mathrm{d}r. \tag{4}$$

Functions $B_j = j\cdot\int_0^{2\pi}((r - R\cos\theta)/D_j^{3/2})\mathrm{d}\theta$ and $C_j = j\cdot\int_0^{2\pi}(d_j/D_j^{3/2})\mathrm{d}\theta$ are the radial and the axial components of the electric field generated by the dipole rings, $D_j = r^2 + d_j^2 + R^2 - 2rR\cos\theta$, where the subscript index $j = -1$ and 1. $d_{-1} = (\mathrm{L} + 1)$ nm and $d_1 = 1$ nm are the distances from the monitor window to the upper or lower ring. Q can be obtained from $Q = P/L = \varepsilon_0\alpha E_0/L$. Thus, the enhancement of the near field, η_m, is

$$\eta_m = \frac{\bar{E}^2}{E_0^2} = \frac{\alpha^2}{64\pi^5 L^2 R^2}\int_0^R \left(\left(\sum\nolimits_j B_j\right)^2 + \left(\sum\nolimits_j C_j\right)^2\right)\cdot 2\pi r\mathrm{d}r. \tag{5}$$

We plot the analytically calculated NFE (η_m) values from Eq. (5) as a function of the monopole antenna radius in Fig. 3(d). We also plot the numerically simulated NFE (η_m) values for the monopole antenna from Fig. 2 into Fig. 3(d), in order to compare the FDTD simulation result with our dipole ring calculation result. Figure 3(d) indicates that the analytical calculation result has a very similar behavior to our numerical simulation result, and both are demonstrating a maximum NFE value as the radius varies. The peak position for the analytical calculation is at $R = 8$ nm, which is very close to the 7 nm peak position of the numerical simulation. However, the values of the analytical calculation are about 1.6 times the values of the FDTD simulation. This quantity difference is due to our approximation in the analytical calculation that all the surface charges accumulate around the rings of the rod ends.

This analytical calculation helps us to understand the physical reason why the size-dependent NFE value has a maximum at a certain radius. The optimization in size is the result of the combination and compromise of two terms, the total radiated energy of the optical antenna and the near-field distribution factor. In Eq. (6) we divide η_m into two parts: η_{m_t}, the total radiated energy of the optical antenna normalized to the incoming field power density, and η_{m_d}, the near-field distribution factor. η_{m_t} is calculated from the power of a dipole $\frac{4\pi^3 c}{3\varepsilon_0\lambda^4}|P|^2$ divided by the incoming field power in a unit volume, $\frac{\varepsilon_0 c|E_0|^2\Omega_0}{2\lambda}$. λ is the incident wavelength, c is the light speed, Ω_0 is the unit volume and is considered as 1 in our calculation. η_{m_d} reflects all the location-related terms.

$$\eta_m = \eta_{m\_t}\cdot\eta_{m\_d}, \qquad \eta_{m\_t} = \frac{8\pi^3}{3\lambda^3\Omega_0}\alpha^2$$
$$\eta_{m\_d} = \frac{3\lambda^3\Omega_0}{512\pi^8 R^2 L^2}\int_0^R \left(\left(\sum\nolimits_j B_j\right)^2 + \left(\sum\nolimits_j C_j\right)^2\right)\cdot 2\pi r\mathrm{d}r, \tag{6}$$

In Fig. 3(f), we plot the η_{m_t} and η_{m_d}, as functions of the antenna radius. η_{m_t} shows a sharp drop in values at the small radius end, because the total radiated energy of the antenna obtained from the incoming excitation field will diminish quickly with decreasing size after $R < 10$ nm. On the other hand, η_{m_d} drops faster than the increasing of the η_{m_t} at the large radius end. Therefore, η_m, the product of the two parts, has a best optimized value somewhere when R is between 1 and 10 nm for an 800-nm excitation, and is a joint result of

the total radiated energy of the antenna and the concentrated distribution factor at the enhancement location.

For the cone-shaped antenna, we use the same method to calculate the antenna polarizability, as we approximately consider the cone to be an ellipsoid with equal volume. The surface charges are considered to accumulate and oscillate around the rings of the end faces and form the dipole ring of the cone-shaped antenna, as Fig. 3(c) shows. The near field is calculated by taking an average of the field in a monitor window, which is a round area ($4R^2$ in size and $1.13R$ in radius) and 1 nm away from the tip end face. The calculated NFE (η_c) values as a function of the antenna tip radius are plotted in Fig. 3(e), and the numerically simulated NFE (η_c) values from Fig. 2 are also plotted for comparison. Our analytical result shows a similar behavior as the numerical simulation for most radii, but departs from numerical simulation at the very small radius end (2 and 3 nm). In terms of absolute values, the ratios of our analytical values and numerical values are smaller than 3. This suggests that our model with the rough ellipsoid approximation is still applicable for cone shapes until the tip size is smaller than 3 nm. The failure at a very small radius does not devalue our method because calculating a feature size smaller than 3 nm is fundamentally difficult with any analytical or numerical classical method.

In Fig. 3(g) we plot the η_{c_t} (the total radiated energy of the cone-shaped antenna normalized to the incoming field power density) and η_{c_d} (the near-field distribution factor), as functions of the antenna radius. Differing from η_{m_t} in Fig. 3(f), the η_{c_t} shows a much (10^3) slower dropping at the small radius end. This is due to the constant size (15-nm radius) at the large end of the cone antenna and the equal volume ellipsoid approximation when we calculate the antenna polarizability. This 10^3 smaller dropping η_{c_t} causes the analytically calculated η_c to continuously increase at the very small radius end. The large end of a cone does help with increasing the total energy the antenna takes from the incident field and transports energy to the small end to increase the field at the tip, however, the transporting efficiency should diminish when the tip gets to be too small. The changing of the plasmon transport efficiency with reducing radius is not considered in our model. The behavior difference at the small radius end in Fig. 3(e) is probably due to the above reason, and weakly suggests that the cutoff radius for efficient plasmon transport on a gold wire is about 3 nm.

4. PHYSICAL MEANINGS AND CONSEQUENCES

Our simulation results in Table 1 and Fig. 2 clearly show that NFE has a strong dependence on and has an optimization condition associated to the nanoantenna's size, although all those antennae satisfy the plasmon resonance condition with the excitation field. These results prove that an optimum size exists for all four investigated types of antennae, which cover single-body, two-body, symmetrical and asymmetrical types. Therefore, the idea of "the smaller the tip, the stronger the enhancement" is not right in general.

Our simulation results for cone-shaped antennae suggest that a finite-sized cone-shaped antenna might be able to improve the enhancement factor by an order of magnitude from current infinite-sized tips. In experiments, people commonly use infinite-sized field enhancement tips, e.g., microsharpened macro-sized metal tips or metal-coated AFM (atomic force microscopy) tips, to perform tip enhanced near-field microscopy. Reported experiments with those tips have shown that a single metal tip setup normally offers a field enhancement factor at the scale of 10^3 and a spatial resolution of 10 nm [27]. For finite-sized cone-shaped antennae, our simulations show that the maximum NFE is at 3 nm and suggests a best tip diameter at 6 nm with a 10^4 enhancement factor. This is half the best resolution and 10 times the maximum enhancement reported from infinite-sized tips. The improvement in enhancement might be due to the plasmon resonance achieved with finite-sized cone-shaped antennae. Such finite-sized cone-shaped tips might be fabricated by depositing a few hundred nanometer metal films on the end of a dielectric rod and sharpening it afterward.

Another conclusion from our study is the maximum potential of a single optical antenna in NFE stands at about 2×10^5 for a linear signal, or 4×10^{10} for typical nonlinear (i.e., $\chi^{(2)}$) signals. The cone-bowtie antenna structure is the best design to offer a high field enhancement, and our FDTD simulation shows that a gold cone-bowtie antenna offers 2×10^5 field enhancement at the best for a linear signal. Another commonly used material, silver, offers a slightly higher enhancement than gold, and the difference is little (less than 50%) [28]. All simulations and calculations in this report are considering only linear processes. Signals from a typical nonlinear measurement, e.g., tip-enhanced spectroscopy or a two-photon excitation measurement, are proportional to the fourth power of the incident electric field or the square of the field enhancement factor we are discussing in this report. Therefore, the maximum potential in signal enhancement for nonlinear signals is about 4×10^{10}. Arrays of antennae are not considered in this report; a multiple antennae structure might further increase the local field enhancement due to constructive interferences.

5. CONCLUSION

Taking into account a fixed working wavelength, we perform numerical simulations for four different kinds of gold nanoantennae—monopole, dipole, cone-shaped, and cone-bowtie antennae—to study the optimization and maximum potential of optical antennae in NFE. The results indicate that the near-field antennae have an optimum size for offering the best enhancement at a certain working wavelength. This conclusion might be applicable to all near-field enhancement antennae and probes, and reveals that seeking methods to manufacture further smaller probes cannot always solve the problem if enhancement is not high enough. Our simulation for cone-shaped antennae shows an order of magnitude higher enhancement than infinite-sized metal tips, and might reveal a way to further improve tip enhancement by fabricating nano-sized cone-shaped antennae. We also present an analytical calculation method, using a distributed dipole ring approximation for monopole and cone-shaped antennae, to evaluate and analyze antenna designs. This method offers significantly reduced calculation time and much better physical insights than numerical methods. It proves that the physical reasons for such

an optimization at a certain size are the combination and compromise of the total radiated energy of the optical antenna and the near-field distribution factor. In terms of the maximum enhancement factor, the simulation result for the gold cone-bowtie antennae sets the values at about 2×10^5 for a linear signal and 4×10^{10} for typical nonlinear signals. These values might represent the maximum potential of the field enhancement of optical antennae, unless a better antenna design can be proposed.

Ministry of Education of the People's Republic of China; National Natural Science Foundation of China (11004231).

Yan Yin acknowledges and thanks helpful discussions with Wei Ding.

REFERENCES

1. K. Kneipp, Y. Wang, H. Kneipp, L. T. Perelman, I. Itzkan, R. Dasari, and M. S. Feld, "Single molecule detection using surface-enhanced Raman scattering (SERS)," Phys. Rev. Lett. **78**, 1667–1670 (1997).
2. S. M. Nie and S. R. Emery, "Probing single molecules and single nanoparticles by surface-enhanced Raman scattering," Science **275**, 1102–1106 (1997).
3. K. D. Alexander, K. Skinner, S. P. Zhang, H. Wei, and R. Lopez, "Tunable SERS in gold nanorod dimers through strain control on an elastomeric substrate," Nano Lett. **10**, 4488–4493 (2010).
4. N. Mishra and G. V. P. Kumar, "Near-field optical analysis of plasmonic nano-probes for top-illumination tip-enhanced Raman scattering," Plasmonics **7**, 359–367 (2012).
5. Z. Y. Li and Y. N. Xia, "Metal nanoparticles with gain toward single-molecule detection by surface-enhanced Raman scattering," Nano Lett. **10**, 243–249 (2010).
6. Z.-Y. Li, "Optics and photonics at nanoscale: principles and perspectives," Europhys. Lett. **110**, 14001–14007 (2015).
7. R. D. Grober, R. J. Schoelkopf, and D. E. Prober, "Optical antenna: towards a unity efficiency near-field optical probe," Appl. Phys. Lett. **70**, 1354–1356 (1997).
8. E. Cubukcu, N. F. Yu, E. J. Smythe, L. Diehl, K. B. Crozier, and F. Capasso, "Plasmonic laser antennas and related devices," IEEE J. Sel. Top. Quantum Electron. **14**, 1448–1461 (2008).
9. S. Kessentini, D. Barchiesi, C. D'Andrea, A. Toma, N. Guillot, E. Di Fabrizio, B. Fazio, O. M. Marago, P. G. Gucciardi, and M. L. de la Chapelle, "Gold dimer nanoantenna with slanted gap for tunable LSPR and improved SERS," J. Phys. Chem. C **118**, 3209–3219 (2014).
10. T. Ye, Y. Gao, and Y. Yin, "Surface-enhanced Raman scattering effects of gold nanorods prepared by polycarbonate membranes," Acta Phys. Sin. **62**, 127801 (2013).
11. A. Downes, D. Salter, and A. Elfick, "Simulations of atomic resolution tip-enhanced optical microscopy," Opt. Express **14**, 11324–11329 (2006).
12. S. S. Kharintsev, G. G. Hoffmann, A. I. Fishman, and M. K. Salakhov, "Plasmonic optical antenna design for performing tip-enhanced Raman spectroscopy and microscopy," J. Phys. D **46**, 145501 (2013).
13. P. Muhlschlegel, H. J. Eisler, O. J. F. Martin, B. Hecht, and D. W. Pohl, "Resonant optical antennas," Science **308**, 1607–1609 (2005).
14. A. Taflove and S. C. Hagness, *Computational Electrodynamics: The Finite-Difference Time-Domain Method* (Artech House, 2005).
15. S. D. Gedney, *Introduction to the Finite-difference Time-domain (FDTD) Method for Electromagnetics* (Morgan & Claypool, 2011).
16. G. W. Bryant, F. J. G. De Abajo, and J. Aizpurua, "Mapping the plasmon resonances of metallic nanoantennas," Nano Lett. **8**, 631–636 (2008).
17. O. Perez-Gonzalez, N. Zabala, and J. Aizpurua, "Optical characterization of charge transfer and bonding dimer plasmons in linked interparticle gaps," New J. Phys. **13**, 83013–83028 (2011).
18. S. Y. Liu, J. F. Li, F. Zhou, L. Gan, and Z. Y. Li, "Efficient surface plasmon amplification from gain-assisted gold nanorods," Opt. Lett. **36**, 1296–1298 (2011).
19. C. F. Bohren and D. R. Huffman, "Particles small compared with the wavelength," in *Absorption and Scattering of Light by Small Particles* (Wiley, 2007), pp. 130–157.
20. R. D. Averitt, S. L. Westcott, and N. J. Halas, "Linear optical properties of gold nanoshells," J. Opt. Soc. Am. B **16**, 1824–1832 (1999).
21. L. B. Scaffardi and J. O. Tocho, "Size dependence of refractive index of gold nanoparticles," Nanotechnology **17**, 1309–1315 (2006).
22. P. B. Johnson and R. W. Christy, "Optical constants of noble metals," Phys. Rev. B **6**, 4370–4379 (1972).
23. V. Myroshnychenko, J. Rodriguez-Fernandez, I. Pastoriza-Santos, A. M. Funston, C. Novo, P. Mulvaney, L. M. Liz-Marzan, and F. J. G. de Abajo, "Modelling the optical response of gold nanoparticles," Chem. Soc. Rev. **37**, 1792–1805 (2008).
24. U. Kreibig and M. Vollmer, *Optical Properties of Metal Clusters* (Springer, 1995).
25. W. Ding, R. Bachelot, R. E. de Lamaestre, D. Macias, A. L. Baudrion, and P. Royer, "Understanding near/far-field engineering of optical dimer antennas through geometry modification," Opt. Express **17**, 21228–21239 (2009).
26. F. Zhou, Z. Y. Li, Y. Liu, and Y. N. Xia, "Quantitative analysis of dipole and quadrupole excitation in the surface plasmon resonance of metal nanoparticles," J. Phys. Chem. C **112**, 20233–20240 (2008).
27. E. J. Sanchez, L. Novotny, and X. S. Xie, "Near-field fluorescence microscopy based on two-photon excitation with metal tips," Phys. Rev. Lett. **82**, 4014–4017 (1999).
28. J. Aizpurua, G. W. Bryant, L. J. Richter, F. J. G. de Abajo, B. K. Kelley, and T. Mallouk, "Optical properties of coupled metallic nanorods for field-enhanced spectroscopy," Phys. Rev. B **71**, 235420 (2005).